A Method for Evaluating Frequency Regulation in an Electrical Grid – Part I: Theory

Federico Milano, *Fellow, IEEE*, Álvaro Ortega, *Member, IEEE*

***Abstract*— The first part of this two-part paper proposes a technique that consists in the measurement, through phasor measurement units, of bus frequency variations to estimate the rate of change of regulated power, and in the definition of a local index that is able to discriminate between devices that modify the frequency at the connection bus and devices that do not. A taxonomy of devices based on their ability to modify locally the frequency is proposed. A byproduct of such an index is to estimate the inertia or equivalent inertia of the monitored device. The proposed index is shown to be a relevant consequence of the concept of *frequency divider formula* recently published by the authors on the IEEE Transactions on Power Systems. The properties of the proposed index is illustrated through examples based on the synchronous machine and its controllers.**

***Index Terms*— Primary frequency control, inertial response, phasor measurement unit (PMU), converter-interfaced generation.**

I. Introduction

A current challenge for the secure operation of the grid is the ability of TSOs to determine through simple measurements whether a device connected to the grid provide frequency control at a given time [1]–[3]. Some TSOs have resolved the problem by measuring the active power output to estimate their mileage. Other TSOs "trust" the operators of power plants, which might expose the system to security issues if the control is not provided or available when needed. A third approach consists in allocating conventional frequency reserve, which guarantees a secure operation but leads to higher energy costs. This paper addresses this problem and provides a theoretical framework for its solution.

The need for metrics to define the frequency response and control in a transmission system has been recognized since a decade ago. The report [4], for example, defines three obvious metrics, namely frequency nadir, nadir-based frequency response, and primary frequency response. These are, however, "global" metrics and are adequate only for off-line adequacy and reliability studies. Existing techniques to evaluate the primary frequency and inertial responses are qualitative and based on statistical analysis of time series [5], [6] or on Kalman filtering [7].

F. Milano is with the AMPSAS research group, School of Elec. and Electron. Eng., University College Dublin, Ireland. Á. Ortega is with **LOYOLA**Tech, Universidad Loyola Andalucía, Spain. E-mails: federico.milano@ucd.ie; aortega@uloyola.es

This material is based upon works supported by the European Commission and the Science Foundation Ireland by funding F. Milano under the Project EdgeFLEX, grant no. 883710, and under the Investigator Programme award, project AMPSAS, grant no. SFI/15/IA/3074, respectively. This work is also supported by the European Commission and by the Spanish Ministry of Science by funding Á. Ortega under projects FLEXITRANSTORE – H2020-LCE-2016-2017-SGS-774407 and ENE2017-88889-C2-1-R, respectively.

The technique proposed in this paper is based exclusively on bus frequency measurements, and is conceptually different from existing approaches as it is local, quantitative and aimed at on-line applications. The proposed approach is a further elaboration on the concept of Frequency Divider Formula (FDF) [8], which has already been utilized to estimate bus frequencies [9], machine rotor speeds [10] and the frequency of the Center of Inertia (CoI) [11].

The first part of this two-part paper provides the following contributions.

- An alternative derivation of the FDF presented in [8]. The new formulation is obtained starting from the expression of the power flow equations and is shown to have formally the same structure than the dc power flow equation.
- A practical criterion to determine whether, in transient conditions, a device provides inertial response and/or frequency control.
- A taxonomy of devices that modify the frequency at their point of connection with the grid for a variety of technologies, including synchronous machines, loads, renewable generation and energy storage systems.
- The dc power-flow based derivation of the FDF leads to relevant byproducts on the impact of a device on frequency variations and on the ability to estimate frequency variations through active power measurements rather than using voltage phasors as commonly implemented in Phase-Locked Loops (PLLs).
- An approximated expression to determine, in transient conditions, the equivalent inertia of a device based on active power and frequency measurements.

Part I also illustrates the main features of the proposed technique through a set of examples that focus on synchronous machines and conventional primary and secondary frequency regulation. In the second part, we extend the analysis to non-synchronous devices and present a statistical approach to evaluate the frequency regulation support provided by non-dispatchable distributed energy resources.

The remainder of Part I of this paper is organized as follows. Section II recalls the formulation of the FDF proposed in [8] and provides an alternative formulation as a derivation of the well-known power flow equations. Section III describes the rationale and the formulation of the proposed index to discriminate between devices that provide inertial response/fast frequency regulation or not. Dynamic state estimation of bus frequencies as well as the approximated expression to estimate, during a transient, the equivalent inertia of a device are discussed in Section IV. A set of illustrative examples based

on the well-known WSCC 9-bus, 3-machine test system is provided in Section V. Finally, a summary of the theoretical results is presented in Section VI.

II. Frequency Divider Formula

In [8], the starting point of the definition of the FDF is the augmented admittance matrix and the relation between current injections and voltages at network buses.

In this section, we first recall the definition of the FDF in Subsection II-A. An alternative derivation of the same formula based on the power flow formulation is then provided in Subsection II-B. An interesting feature of the proposed formulation is its formal similarity with the well known dc power flow formulation [12], [13]. It is important to note, however that this similarity is only formal, as the proposed formulation is actually not an approximation of the power flow equations but, rather, represent a part of it, which, in this paper, we call *regulating power*. The two formulations of the FDF are complementary and will be used later in the paper to show the properties of devices that modify, locally, the frequency by providing either inertial or fast frequency response, and to derive an expression to estimate inertia.

A. Derivation based on current injections

For the determination of the FDF in [8] we utilized the augmented admittance matrix, which includes the network connections and electromotive forces (emfs) behind the internal reactances of the synchronous machines (SMs), as follows:

$$\begin{bmatrix} \bar{\boldsymbol{i}}_{\mathrm{G}}(t) \\ \bar{\boldsymbol{i}}_{\mathrm{B}}(t) \end{bmatrix} = \begin{bmatrix} \bar{\mathbf{Y}}_{\mathrm{GG}} & \bar{\mathbf{Y}}_{\mathrm{GB}} \\ \bar{\mathbf{Y}}_{\mathrm{BG}} & \bar{\mathbf{Y}}_{\mathrm{BB}} \end{bmatrix} \begin{bmatrix} \bar{\boldsymbol{e}}_{\mathrm{G}}(t) \\ \bar{\boldsymbol{v}}_{\mathrm{B}}(t) \end{bmatrix} , \tag{1}$$

where the subscripts G and B stand for synchronous generation buses, and for load and transition buses, respectively; $\bar{\boldsymbol{v}}_{\mathrm{B}}(t)$ and $\bar{\boldsymbol{i}}_{\mathrm{B}}(t)$ are bus voltages and current injections, respectively, at network buses; $\bar{\boldsymbol{i}}_{\mathrm{G}}(t)$ are generator current injections; $\bar{\boldsymbol{e}}_{\mathrm{G}}(t)$ are generator emfs behind the internal generator impedance; $\bar{\mathbf{Y}}_{\mathrm{GG}} \in \mathbb{C}^{m\times m}$; $\bar{\mathbf{Y}}_{\mathrm{BB}} \in \mathbb{C}^{n\times n}$; $\bar{\mathbf{Y}}_{\mathrm{GB}} \in \mathbb{C}^{m\times n}$; and $\bar{\mathbf{Y}}_{\mathrm{BG}} \in \mathbb{C}^{n\times m}$. The sub-matrix $\bar{\mathbf{Y}}_{\mathrm{BB}}$ is:

$$\bar{\mathbf{Y}}_{\mathrm{BB}} = \bar{\mathbf{Y}}_{\mathrm{bus}} + \bar{\mathbf{Y}}_{\mathrm{G}} , \tag{2}$$

where $\bar{\mathbf{Y}}_{\mathrm{bus}}$ is the well-known network admittance matrix, and $\bar{\mathbf{Y}}_{\mathrm{G}}$ is a diagonal matrix whose h-th diagonal element is 0 if no machine is connected to bus h, and the inverse of $jx_{\mathrm{G},h}$ if such a machine is connected to bus h, where $x_{\mathrm{G},h}$ is the machine internal transient reactance. $x_{\mathrm{G},h}$ also includes the reactance of the step-up transformer of the machine if this is not part of the network topology.

Assuming negligible the contribution of load currents (as commonly done in fault analysis), the relationship between bus voltages $\bar{\boldsymbol{v}}_{\mathrm{B}}(t)$ and emfs $\bar{\boldsymbol{e}}_{\mathrm{G}}(t)$ can be written as:

$$\bar{\mathbf{Y}}_{\mathrm{BG}}\bar{\boldsymbol{e}}_{\mathrm{G}}(t) = -\bar{\mathbf{Y}}_{\mathrm{BB}}\bar{\boldsymbol{v}}_{\mathrm{B}}(t) . \tag{3}$$

Differentiating (3) with respect to time and applying the simplifications discussed in [8], the FDF is obtained as:

$$\mathbf{B}_{\mathrm{BG}}\Delta\boldsymbol{\omega}_{\mathrm{G}}(t) = -\mathbf{B}_{\mathrm{BB}}\Delta\boldsymbol{\omega}_{\mathrm{B}}(t) , \tag{4}$$

where $\Delta\boldsymbol{\omega}_{\mathrm{G}}(t) \in \mathbb{R}^m$ is the vector of machine rotor speed variations; $\Delta\boldsymbol{\omega}_{\mathrm{B}}(t) \in \mathbb{R}^n$ are the frequency variations at the system buses; and $\mathbf{B}_{\mathrm{BG}} = \mathrm{Im}\{\bar{\mathbf{Y}}_{\mathrm{BG}}\}$ and $\mathbf{B}_{\mathrm{BB}} = \mathrm{Im}\{\bar{\mathbf{Y}}_{\mathrm{BB}}\}$, where $\mathbf{B}_{\mathrm{BB}}$ has same rank and symmetry properties as $\bar{\mathbf{Y}}_{\mathrm{BB}}$. In (4), frequency variations are in per unit with respect to the system reference frequency.

B. Derivation based on power flow formulation

The complex power injection at the network buses of the system, say $\bar{\boldsymbol{s}}_{\mathrm{B}}$, can be expressed in terms of the well-known power flow equations, as follows:

$$\bar{\boldsymbol{s}}_{\mathrm{B}}(t) = \boldsymbol{p}_{\mathrm{B}}(t) + j\boldsymbol{q}_{\mathrm{B}}(t) = \bar{\boldsymbol{v}}_{\mathrm{B}}(t) \circ \left[\bar{\mathbf{Y}}^{*}_{\mathrm{bus}}\,\bar{\boldsymbol{v}}^{*}_{\mathrm{B}}(t)\right] , \tag{5}$$

where $\circ$ is the Hadamard product, i.e., the element-by-element product by two vectors. For the sake of the derivation, it is convenient to rewrite (5) in an element-wise notation and extract the active power:

$$\begin{aligned} p_{\mathrm{B},h}(t) = {} & v_{\mathrm{B},h}(t) \sum_{k\in\mathbb{B}} v_{\mathrm{B},k}(t)\, G^{hk}_{\mathrm{bus}}\, \cos\theta_{\mathrm{B},hk}(t) \\ & + v_{\mathrm{B},h}(t) \sum_{k\in\mathbb{B}} v_{\mathrm{B},k}(t)\, B^{hk}_{\mathrm{bus}}\, \sin\theta_{\mathrm{B},hk}(t) , \end{aligned} \tag{6}$$

where $\mathbb{B}$ is the set of network buses; G^{hk}_{bus} and B^{hk}_{bus} are the real and imaginary parts of the element (h,k) of the network admittance matrix, i.e. $\bar{Y}^{hk}_{\mathrm{bus}} = G^{hk}_{\mathrm{bus}} + jB^{hk}_{\mathrm{bus}}$; $v_{\mathrm{B},h}$ and $v_{\mathrm{B},k}$ denote the voltage magnitudes at buses h and k, respectively; and $\theta_{\mathrm{B},hk}(t) = \theta_{\mathrm{B},h}(t) - \theta_{\mathrm{B},k}(t)$, where $\theta_{\mathrm{B},h}(t)$ and $\theta_{\mathrm{B},k}(t)$ are the voltage phase angles at buses h and k, respectively.

Let us differentiate (7) and write the active power injections as the sum of two components:

$$\begin{aligned} dp_{\mathrm{B},h} &= \sum_{k\in\mathbb{B}} \frac{\partial p_{\mathrm{B},h}}{\partial\theta_{\mathrm{B},k}}\, d\theta_{\mathrm{B},k} + \sum_{k\in\mathbb{B}} \frac{\partial p_{\mathrm{B},h}}{\partial v_{\mathrm{B},k}}\, dv_{\mathrm{B},k} \\ &= dp'_{\mathrm{B},h} + dp''_{\mathrm{B},h} , \end{aligned} \tag{7}$$

In (7), $dp_{\mathrm{B},h}$ is the total variation of power at bus h, while $dp'_{\mathrm{B},h}$ is what, in the paper, we call "regulating power". In general, $dp_{\mathrm{B},h} \neq dp'_{\mathrm{B},h}$, so $p'_{\mathrm{B},h}(t)$ cannot be measured directly, except for some special cases that are discussed in Section III. This is why an approach to determine $p'_{\mathrm{B},h}(t)$ indirectly based on frequency measurements is proposed in this paper. The second term in (7), namely $p''_{\mathrm{B},h}(t)$, by definition, does not depend on phase angle variations and thus plays no role in altering the frequency of the buses and thus is not further considered in the remainder of this paper. As a matter of fact, it appears that $p''_{\mathrm{B},h}(t)$ is the quota of the active power that behaves as a passive admittance. The rationale of this statement is provided in the Appendix and further illustrated through the numerical examples discussed in Subsection IV-A of Part II.

While one can use the expression of $dp'_{\mathrm{B},h}$ as is, i.e., as a nonlinear function of voltage magnitudes and phase angles, we have observed that the dependency on such quantities can be simplified without compromising its accuracy as follows.

- The first term in (7), namely $dp'_{\mathrm{B},h}$, is the one that varies the most when the active power at bus h is regulated, whereas the contribution to the active power regulation

of the second term, namely $dp''_{\mathrm{B},h}$, is negligible, if any at all.

- The differentiation of $dp'_{\mathrm{B},h}$ with respect to time can be conveniently approximated with:

$$\dot{p}'_{\mathrm{B},h}(t) \approx \Omega_b \sum_{k\in\mathbb{B}} B^{hk}_{\mathrm{bus}}\, \omega_{\mathrm{B},k}(t) \ , \tag{8}$$

where $\omega_{\mathrm{B},k}(t) = \Omega_b^{-1}\dot{\theta}_{\mathrm{B},k}(t)$ is the frequency in pu(rad/s) at bus k; Ω_b is the reference synchronous speed in rad/s;[1] and where it is assumed:

$$\frac{\partial p'_{\mathrm{B},h}}{\partial \theta_{\mathrm{B},k}} \approx B^{hk}_{\mathrm{bus}} \, . \tag{9}$$

The two assumptions above have been thoroughly tested considering:

- Several networks of different size (from three to thousands of buses) and topology (both transmission and distribution systems);
- A large variety of devices ranging from conventional synchronous machines and loads to non-synchronous generators based on wind and solar as well as converter-based energy storage systems with and without frequency control.
- A variety of faults and large disturbances, including three-phase faults, and device outages (please see also Part II of this paper).

In all cases, the approximation assumed in (9) has proven to be extremely good, which leads to conclude that the effect of voltage magnitudes is effectively negligible, if any at all. Therefore, the accuracy and effectiveness of the approach proposed in the paper have been confidently proven.

Note that from (9), the time integral of (8) can be approximated (without loss of accuracy) as:

$$p'_{\mathrm{B},h}(t) \approx \sum_{k\in\mathbb{B}} B^{hk}_{\mathrm{bus}} \theta_{\mathrm{B},k}(t) \, , \tag{10}$$

or, recovering the vector-based notation:

$$\boldsymbol{p}'_{\mathrm{B}}(t) = -\mathbf{B}_{\mathrm{bus}} \boldsymbol{\theta}_{\mathrm{B}}(t) \, , \tag{11}$$

which appears to have the same formal expression as the well-known dc power flow formulation [12]. It is important to note, however, that in the dc power flow the term on the left-hand side of the equation is the *total* power. Instead and crucial for the development of this paper and its companion Part II, in (11), the term on the left-hand side is only a quota of the active power, i.e., the regulating power $\boldsymbol{p}'_{\mathrm{B}}(t)$.

Differentiating (11) with respect to time gives the most important equation this paper, which in turn is the vector-based notation of (8), namely:

$$\boxed{\dot{\boldsymbol{p}}'_{\mathrm{B}}(t) = -\Omega_b \mathbf{B}_{\mathrm{bus}} \Delta\boldsymbol{\omega}_{\mathrm{B}}(t) = -\hat{\mathbf{B}}_{\mathrm{bus}} \Delta\boldsymbol{\omega}_{\mathrm{B}}(t)} \ , \tag{12}$$

The vector $\dot{\boldsymbol{p}}'_{\mathrm{B}}(t)$ represents the Rate of Change of Power (RoCoP) injections into the generator nodes. It is important to reiterate that this quantity is not trivially the numerical derivative of the active power injection/consumption at network buses as $\boldsymbol{p}_{\mathrm{B}}(t) = \boldsymbol{p}'_{\mathrm{B}}(t) + \boldsymbol{p}''_{\mathrm{B}}(t)$ and, in general, $\boldsymbol{p}''_{\mathrm{B}}(t) \neq 0 \ \forall t$.

To complete this section, it remains to show that the frequency divider formula (4) can be derived from (12), and that (12) is actually a generalization of (4). With this aim, we need an additional step. Matrix $\mathbf{B}_{\mathrm{BB}}$ can be obtained from $\mathbf{B}_{\mathrm{bus}}$ as follows:

$$\mathbf{B}_{\mathrm{BB}} = \mathbf{B}_{\mathrm{bus}} + \mathbf{B}_{\mathrm{G}} \ , \tag{13}$$

where $\mathbf{B}_{\mathrm{G}}$ is a diagonal matrix where the h-th element is either $-1/x_{\mathrm{G},h}$, or 0 if no generator is connected to bus h. Merging together (4), (12) and (13), we obtain:[2]

$$\dot{\boldsymbol{p}}'_{\mathrm{B}}(t) = \Omega_b [\mathbf{B}_{\mathrm{BG}} \Delta\boldsymbol{\omega}_{\mathrm{G}}(t) + \mathbf{B}_{\mathrm{G}} \Delta\boldsymbol{\omega}_{\mathrm{B}}(t)] \ , \tag{14}$$

or, equivalently

$$\dot{\boldsymbol{p}}'_{\mathrm{B}}(t) = \hat{\mathbf{B}}_{\mathrm{BG}} \left[\Delta\boldsymbol{\omega}_{\mathrm{G}}(t) - \Delta\boldsymbol{\omega}_{\mathrm{BG}}(t)\right] \ , \tag{15}$$

or, equivalently:

$$\mathbf{B}_{\mathrm{BG}} \left[\Delta\boldsymbol{\omega}_{\mathrm{G}}(t) - \Delta\boldsymbol{\omega}_{\mathrm{BG}}(t)\right] = -\mathbf{B}_{\mathrm{bus}} \Delta\boldsymbol{\omega}_{\mathrm{B}}(t) \ , \tag{16}$$

where $\Delta\boldsymbol{\omega}_{\mathrm{BG}}(t) \subset \Delta\boldsymbol{\omega}_{\mathrm{B}}(t)$ is the subset of frequency deviations at the terminal buses of the SMs.

Expressions (12) and (15) indicate that a time-varying active power injection into the network bus modifies the frequency at that bus. Noteworthy, such active power variation can be originated by device other than just SMs. This concept is further elaborated in the remainder of the paper.

III. Taxonomy of Devices based on the RoCoP

The observation that motivates this paper originates from the structure of the revisited FDF given in (16). First, let us consider the simple example of Fig. 1, where an SM is connected in antenna with the grid through a transmission line.[3] In this example the step-up transformer is included in the machine model, hence $x_{\mathrm{G}} = x'_{\mathrm{d}} + x_{\mathrm{T}}$.

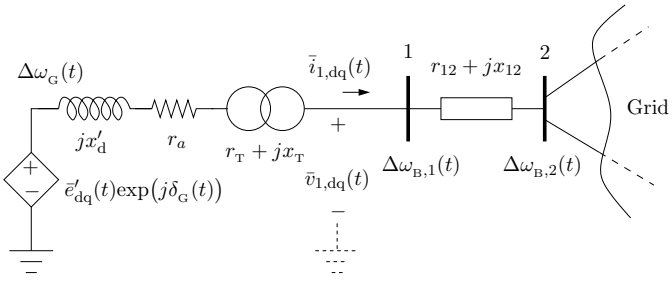

Fig. 1: Synchronous machine connected in antenna to the grid.

In Fig. 1, bus 1 is the terminal bus of the generator that is accessible and "measurable" by the TSO, whereas bus 2 is the high-voltage neighboring bus at the receiving end of the transmission line that connects the generator to the rest of the grid. Note that the step-up transformer could be also used

[1] Multiplying the right-hand side of (8) by Ω_b is necessary to take into account the fact that the phase angles $\theta_{\mathrm{B},k}$ are in radians, while $\omega_{\mathrm{B},k}$ are expressed in per unit.

[2] The values of the non-zero elements of each row of $\mathbf{B}_{\mathrm{BG}}$ and $\mathbf{B}_{\mathrm{G}}$ have same magnitude but opposite signs.

[3] The antenna configuration is used for simplicity but, in fact, any topology can be used. The general case is considered in (20).

as the "antenna" connection, provided that both windings are measurable by the TSO. The developments discussed in this section are valid independently on how the step-up transformer is modeled, either internally to the machine or externally as part of the grid.

Applying (16) to bus 1 of the scheme of Fig. 1 leads to:

$$b_{\mathrm{G}}[\Delta\omega_{\mathrm{G}}(t) - \Delta\omega_{\mathrm{B},1}(t)] = (b_{12} + b_{10})\Delta\omega_{\mathrm{B},1}(t) - b_{12}\Delta\omega_{\mathrm{B},2}(t) \ , \tag{17}$$

where $b_{\mathrm{G}} = 1/x_{\mathrm{G}}$ is the internal susceptance of the SM and step-up transformer; b_{10} is the shunt susceptance at bus 1 and $b_{12} = 1/x_{12}$ is the susceptance of the branch that connects buses 1 and 2. In (17), the signs are a consequence of (16) and of assuming b_{G} and b_{12} to be positive if inductive.

Equation (17) is written with the knowledge that the device connected to bus 1 is an SM, which imposes the frequency at the emf behind the susceptance b_{G}. Moreover, for simplicity, we only consider the topology illustrated in Fig. 1. The properties of devices that do and do not modify locally the frequency discussed below, in fact, do not depend on the number of connections of such devices to the grid. The case of multiple connections can be readily taken into account and, as a matter of fact, a general topology is considered for the RoCoP definition given in (20).

Let us now assume that we do not know anything of the device connected to bus 1 (*black box*) but some measurements at its terminal bus. This case is shown in Fig. 2.

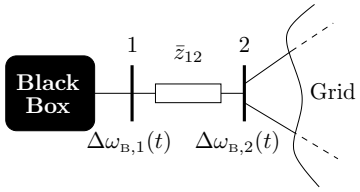

Fig. 2: Black-box device connected in antenna to the grid.

Regardless of the actual behavior of the black box, we can rewrite (17) by assuming that the black box has an internal frequency, $\Delta\omega_{\blacksquare}(t)$, and an equivalent, possibly time-variant susceptance, $b_{\blacksquare}(t)$, both unknown:

$$b_{\blacksquare}(t)[\Delta\omega_{\blacksquare}(t) - \Delta\omega_{\mathrm{B},1}(t)] = b_{12}[\Delta\omega_{\mathrm{B},1}(t) - \Delta\omega_{\mathrm{B},2}(t)] \ , \tag{18}$$

where, consistently with the assumptions that lead to the FDF and without loss of generality, $b_{12} \gg b_{10}$ is assumed. The term $b_{\blacksquare}(t)[\Delta\omega_{\blacksquare}(t) - \Delta\omega_{\mathrm{B},1}(t)]$ in (18) is not known. According to (15), (18) can be also written as:

$$\dot{p}'_{\mathrm{B},1}(t) = \hat{b}_{12}\left[\Delta\omega_{\mathrm{B},1}(t) - \Delta\omega_{\mathrm{B},2}(t)\right] \ , \tag{19}$$

where $\hat{b}_{12} = \Omega_b b_{12}$ and $\dot{p}'_{\mathrm{B},1}(t)$ is the RoCoP at the bus of connection of the black-box device with the grid.

Expression (19) can be conveniently generalized by assuming that there is more than one branch connected to the monitored bus. Hence, assuming to monitor the h-th bus, the proposed general formula to discriminate between devices that modify the frequency at their point of connection and devices that do not is:

$$\boxed{\dot{p}'_{\mathrm{B},h}(t) = \sum_{k\in\mathbb{B}} \hat{b}_{hk}\left[\Delta\omega_{\mathrm{B},h}(t) - \Delta\omega_{\mathrm{B},k}(t)\right]} \ , \tag{20}$$

where $\mathbb{B}$ is the set of buses connected to bus h and b_{hk} is the susceptance of the branch connecting bus h to bus k. Equation (20) only requires the knowledge of the system admittance matrix and the measurement/estimation of the frequencies at the neighboring buses of the device to be monitored. This information is easily available to the TSOs. No confidential information about the device itself has to be provided.

In (20), the term $\sum_{k\in\mathbb{B}} \hat{b}_{hk}\Delta\omega_{\mathrm{B},h}(t)$ represents the combined effect on the frequency of both the device connected to bus h and the rest of the network; whereas the term $\sum_{k\in\mathbb{B}} \hat{b}_{hk}\Delta\omega_{\mathrm{B},k}(t)$ represents the effect of the whole network on the frequency at bus h. Subtracting the latter to the former, what remains is the effect of the black-box device on the frequency variation at bus h.

Next, we discuss some special cases of (20), and provide a taxonomy of devices based on their ability to modify the frequency at their connection point.

A. Devices that Do Not Modify the Frequency

According to our definition, the devices that are unable to modify the frequency at their point of connection satisfy the condition $\dot{p}'_{\mathrm{B},h}(t) = 0, \forall t$, because, by construction of the FDF, there cannot be any variation of frequency within a passive circuit (boundary conditions on the frequency are imposed externally from the device). For such devices, thus, the following relationship holds:

$$\Delta\omega_{\blacksquare,h}(t) \equiv \Delta\omega_{\mathrm{B},h}(t) \ , \ \forall t \ . \tag{21}$$

Constant admittance loads fall in this category. However, for most devices, the condition $\dot{p}'_{\mathrm{B},h}(t) = 0$ is too strict. We thus relax it and assume that a device is unable to modify the frequency at its point of connection if it satisfies the condition:

$$|\dot{p}'_{\mathrm{B},h}(t)| \approx \left|\frac{\Delta p_{\mathrm{B},h}(t)}{\Delta t}\right| < \epsilon \ , \tag{22}$$

where $\epsilon > 0$ is a given empirical threshold that, once agreed upon by all parties, can be used by the TSO to define network codes and ancillary services. A discussion on how to evaluate this threshold in practice is given in Part II.

Condition (22) can be satisfied in two relevant cases:

1) Slow power variations: The device does vary its power consumption/production, but the RoCoP is small in the considered time frame of primary frequency control. According to the notation of (22), this situation is characterized by a non-negligible $\Delta p_{\mathrm{B},h}(t)$ and a *large* Δt. For instance, the secondary frequency control or the daily ramp-up of loads do not significantly vary the frequency at the buses.

2) Small power variations: No load consumption or generation is ever perfectly constant. Stochastic white noise, at least, creates local tiny fluctuations. If the noise is small enough, however, such variations are unable to impact on the frequency. According to the notation of (22), this situation is characterized by *small* $\Delta p_{\mathrm{B},h}(t)$ per unit of time.

In the Appendix, we show that constant admittance loads have $\dot{p}'_{\mathrm{B},h}(t) = 0 \ \forall t$. For nonlinear loads, this condition does not hold in general. However, independently from the load voltage dependency, we can assume that a load can be modelled as two components, one slowly time-varying ramp, $p_{\mathrm{ramp}}(t)$, and a stochastic component, $p_{\mathrm{stoch}}(t)$ (see, for example, the model described in [14]), one has:

$$p_{\mathrm{L}}(t) = p_{\mathrm{ramp}}(t) + p_{\mathrm{stoch}}(t) \ , \tag{23}$$

then $\dot{p}_{\mathrm{L}}(t)$ will be negligible, even though the load consumption is not perfectly constant. The simulation results and discussions presented in Part II of this paper support this conclusion.

B. Devices that Modify the Frequency

According to our definition, a device is able to vary the local frequency whenever the condition $\dot{p}'_{\mathrm{B},h}(t) \neq 0$ holds. Following the discussion above, the only variations of power of interest are those that are sufficiently big to be able to vary the local frequency above a certain threshold and sufficiently fast to be comparable to the time scale of the inertial response and primary frequency control of SMs.

Using the same notation as in (22), a device is able to modify the frequency at its bus of connection if the following condition is satisfied:

$$|\dot{p}'_{\mathrm{B},h}(t)| \approx \left| \frac{\Delta p_{\mathrm{B},h}(t)}{\Delta t} \right| \geq \epsilon \ . \tag{24}$$

In the following, we consider various technologies.

1) Synchronous machines: The dynamics of the rotor speed of a machine connected to bus h can be approximated by:

$$M_{\mathrm{G}} \dot{\omega}_{\mathrm{G}}(t) = p_m(t) - p_{\mathrm{B},h}(t) \ , \tag{25}$$

where M_{G} is the inertia constant and $p_m(t)$ is the mechanical power provided by the turbine. The mechanical power can be decomposed into three terms:

$$p_m(t) = p_{\mathrm{UC}}(t) + p_{\mathrm{PFC}}(t) + p_{\mathrm{AGC}}(t) \ , \tag{26}$$

where $p_{\mathrm{UC}}(t)$ is the power set point as defined by the solution of the unit commitment problem; $p_{\mathrm{PFC}}(t)$ is the regulating power due to primary frequency control (turbine governor) of the machine; and $p_{\mathrm{AGC}}(t)$ is the regulating power due to the secondary frequency control if any, and if the machine participates to it. Hence, the active power injected by an SM into its terminal bus can be written as:

$$p_{\mathrm{B},h}(t) = p_{\mathrm{UC}}(t) + p_{\mathrm{PFC}}(t) + p_{\mathrm{AGC}}(t) - M_{\mathrm{G}} \dot{\omega}_{\mathrm{G}}(t) \ , \tag{27}$$

where $p_{\mathrm{UC}}(t)$ is piece-wise constant and $p_{\mathrm{AGC}}(t)$ varies slowly. Hence, of the four components above, the ones that actually contribute to modify the frequency at the machine bus are $p_{\mathrm{PFC}}(t)$ and the machine inertial response. Therefore:

$$\dot{p}'_{\mathrm{B},h}(t) \approx \dot{p}_{\mathrm{PFC}}(t) - M_{\mathrm{G}} \ddot{\omega}_{\mathrm{G}}(t) \ . \tag{28}$$

In the very first instants after a contingency the dominant effect is due to the inertial response but, in general, the two terms are intertwined. Note, however, that if a machine does not provide primary frequency control, then the lack of regulation can be inferred by observing the transient behavior of $\dot{p}'_{\mathrm{B},h}(t)$, as illustrated in the examples of Section V.

2) Non-synchronous devices regulating the frequency: This category includes, but not limited to, grid-forming power electronics converters of non-synchronous generation and energy storage systems, and thermostatically controlled loads. Such devices consist of a frequency control loop, with a given reference frequency, ω^{ref}, as illustrated in Fig. 3.

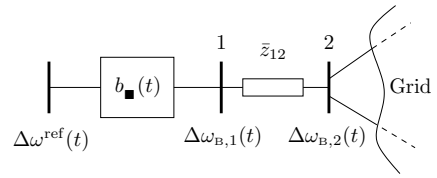

Fig. 3: Example of a device that controls the frequency at bus 1.

The actual implementation of the controller, which is accounted for with a time-dependent susceptance, $b_{\blacksquare}(t)$, is unknown. However, regardless of its transfer function, the controller tracks a reference frequency, so, in turn, $\Delta\omega_{\blacksquare,h}(t) = \Delta\omega^{\mathrm{ref}}(t)$. In practice, ω^{ref} is constant and, hence, $\Delta\omega^{\mathrm{ref}} = 0$. While not known in detail, we can assume that $b_{\blacksquare}(t) \neq 0$ and $\dot{p}'_{\mathrm{B},h}(t) \neq 0$ for any transient condition for which $\Delta\omega_{\mathrm{B},h}(t) \neq \Delta\omega^{\mathrm{ref}}$.

Note that synchronous machines also fall in the category of the frequency controlled device shown in Fig. 3 as conventional generators generally include a turbine governor and provide primary frequency regulation. However, we have discussed synchronous machines separately as they are a relevant special case that will be further discussed in Subsection IV-C.

Next, we present two relevant cases: (i) wind turbines with frequency control, and (ii) energy storage systems.

For a wind turbine, one has:

$$p_{\mathrm{B},h}(t) = p_{\mathrm{stoch}}(t) + p_{\mathrm{PFC}}(t) \ , \tag{29}$$

where the stochastic term $p_{\mathrm{stoch}}(t)$ depends on the uncertainty and volatility of the wind speed and the second term $p_{\mathrm{PFC}}(t)$ is given by the primary frequency controller of the wind turbine, if any. Large and fast stochastic variations, such as wind gusts, are indistinguishable, in principle, from power variations aimed at regulating the frequency. The only difference is statistical. Wind gusts, in fact, will show for about 50% of the times a variation that further increases the actual frequency deviation. Instead, a power variation imposed by a frequency controller always aims at tracking the synchronous frequency. Wind gusts, however, are relatively uncommon and, very often, wind power plants are not operated at their maximum capacity.[4] Moreover, typical values of the autocorrelation coefficients of wind speeds (see, for example, [16]) lead to conclude that wind turbulences have a small local effect on active power fluctuations, whereas the average value of the wind varies quite slowly with time. Thus, except for rare strong wind gusts, the RoCoP of a wind turbine can be assumed to be:

$$\dot{p}'_{\mathrm{B},h}(t) \approx \dot{p}_{\mathrm{stoch}}(t) + \dot{p}_{\mathrm{PFC}}(t) \approx \dot{p}_{\mathrm{PFC}}(t) \ , \tag{30}$$

[4]See, for example, the so-called "wind dispatch down" periods defined by EirGrid and SONI, that effectively make constant the power production of a wind power plant [15].

at least for all variations such that $|\dot{p}'_{\mathrm{B},h}(t)| > \epsilon_{\mathrm{WT}}$, where the threshold ϵ_{WT} can be chosen based on statistical properties (shape factor and autocorrelation) of the wind at the location of the wind power plant. This important point is thoroughly discussed in Part II.

The case of energy storage systems is probably the easiest one to analyze. These devices are based on deterministic controllers and, when used to provide primary frequency support, they generate/absorb power only if the frequency is outside a band around the synchronous reference speed:

$$p_{\mathrm{B},h}(t) = p_{\mathrm{PFC}}(t) \quad \Rightarrow \quad \dot{p}'_{\mathrm{B},h}(t) = \dot{p}_{\mathrm{PFC}}(t) \ . \tag{31}$$

IV. Dynamic State Estimation

This section discusses the consequences of (12) and (20) for the dynamic state estimation of bus frequencies (Subsection IV-A) and machine rotor speeds (Subsection IV-B), as well as an approximated expression to estimate the equivalent inertia of a device, valid in transient conditions (Subsection IV-C).

A. Bus Frequencies

The estimation of bus frequencies is conventionally based on the measurements of bus voltage phasors and the proper design of PLLs, which are part of Phasor Measurement Units (PMUs) or equivalent devices. To achieve a satisfactory level of accuracy with this type of estimation is possible but challenging [17].

Expression (12) suggests that active power measurements can be utilized to estimate frequency variations at network buses. From (12), one has:

$$\Delta\boldsymbol{\omega}_{\mathrm{B}}(t) = \hat{\mathbf{B}}_{\mathrm{bus}}^{-1}\, \dot{\boldsymbol{p}}'_{\mathrm{B}}(t) \ , \tag{32}$$

where $\dot{\boldsymbol{p}}'_{\mathrm{B}}(t)$ can also be approximated with $\Delta\boldsymbol{p}_{\mathrm{B}}/\Delta t$ in a given finite time Δt. *Vice versa*, based on (20), if frequency estimations at network buses are known, the regulating power provided by a device can be estimated as:

$$\Delta p'_{\mathrm{B},h}(t) = \int_t \sum_{k\in\mathbb{B}} \hat{b}_{hk} \left[\Delta\omega_{\mathrm{B},h}(\tau) - \Delta\omega_{\mathrm{B},k}(\tau)\right] d\tau \ . \tag{33}$$

B. Machine Rotor Speed

In [10], we have described how to estimate the rotor speeds of SMs based on (4). The noteworthy result of [10] is that such an estimation can be achieved with a reduced set of bus frequency estimations and a linear optimization problem. Considering the example of Fig. 1, the rotor speed of the machine can be obtained as:

$$\Delta\omega_{\mathrm{G}}(t) = \frac{b_{12}+b_{\mathrm{G}}}{b_{\mathrm{G}}}\, \Delta\omega_{\mathrm{B},1}(t) - \frac{b_{12}}{b_{\mathrm{G}}}\, \Delta\omega_{\mathrm{B},2}(t) \ . \tag{34}$$

Equation (15) leads to an alternative expression to estimate the rotor speed of the machine based only on measurements at the terminal bus of the machine itself (thus also eliminating the issue of measurement delays discussed in [10]):

$$\Delta\omega_{\mathrm{G}}(t) = \Delta\omega_{\mathrm{B},1}(t) - \hat{x}_{\mathrm{G}}\dot{p}'_{\mathrm{B},1}(t) \ , \tag{35}$$

where $\hat{x}_{\mathrm{G}} = 1/\hat{b}_{\mathrm{G}}$. The former expression can be also used for any radial connection, such as a long transmission line, to estimate the frequency at one end by measuring the frequency and the active power injection into the other end.

C. Inertia

Elaborating on (28), we can derive an expression to estimate the inertia of an SM or, more interestingly, to estimate the *equivalent* inertia of any non-synchronous device in the transient following a contingency.

The time scale of the inertial response of the machine is faster than that of its primary frequency control. Thus, in the first seconds after an event that causes a power unbalance in the system, we can assume that:

$$\dot{p}_{\mathrm{PFC}}(t) \ll M_{\mathrm{G}}\ddot{\omega}_{\mathrm{G}}(t) \ . \tag{36}$$

Using (36), (28) can be rewritten as:

$$M_{\mathrm{G}}\ddot{\omega}_{\mathrm{G}}(t) \approx -\dot{p}'_{\mathrm{B},h}(t), \quad \text{for } 0 < t < t^* \ , \tag{37}$$

with $t^* \approx 1$ s. Referring again to Fig. 1 and substituting $\ddot{\omega}_{\mathrm{G}}(t)$ with the second time derivative of the expression obtained from (35), (37) becomes:

$$M_{\mathrm{G}}(t) \approx \frac{-\dot{p}'_{\mathrm{B},1}(t)}{d^2/dt^2\left[\Delta\omega_{\mathrm{B},1}(t) - \hat{x}_{\mathrm{G}}\dot{p}'_{\mathrm{B},1}(t)\right]}, \text{ for } t < t^* \ . \tag{38}$$

Equation (38) determines the physical inertia of SMs if applied in the proper time scale.[5] Interestingly, the device to be monitored does not have to be an SM. Equation (38) can be rewritten as an estimation of the *equivalent* inertia that a device connected at bus i shows after a contingency, as follows:

$$\boxed{M_{\blacksquare,h}(t) \approx \frac{-\dot{p}'_{\mathrm{B},h}(t)}{d^2/dt^2\left[\Delta\omega_{\mathrm{B},h}(t) - \hat{x}_{\blacksquare,h}\dot{p}'_{\mathrm{B},h}(t)\right]}, \text{ for } t < t^*} \ , \tag{39}$$

where the parameter $\hat{x}_{\blacksquare,h}$ can be defined for non-synchronous devices based on the nominal power capacity of the device and using typical values for SMs of the same size. Clearly, the device does not need to have a physical inertia. To show $M_{\blacksquare,h}(t) \neq 0$, in fact, the device can provide an inertia-like response through proper fast frequency control. For example, power electronic converters can provide primary frequency control much faster than SMs, thus overlapping the time scale of the inertial response. Equation (39) can thus be utilized by system operators to evaluate and reward as an ancillary service the equivalent "inertial response" of non-synchronous devices.

In steady state, the denominator of equation (39) is null as $\Delta\omega_{\mathrm{B},h}(t) = \dot{p}'_{\mathrm{B},h}(t) = 0$. This is consistent as (39) applies only in transient conditions. However, it is also possible that, during a transient, $\Delta\omega_{\mathrm{B},h}(t) = \hat{x}_{\blacksquare,h}\,\dot{p}'_{\mathrm{B},h}(t) \neq 0$, thus leading to a singularity. This point is further discussed in Section IV-B of Part II.

V. Illustrative Examples

This section presents some illustrative examples based on the well-known WSCC 9-bus system shown in Fig. 4. This network includes 3 SMs (modeled with a fourth order, one direct- and one quadrature-axis machine model), loads (modeled as constant admittances during transients, and as constant power injections in quasi-steady-state conditions) and transformers,

[5] M_{G} is the machine 'starting time,' which is twice the inertia, i.e., $M_{\mathrm{G}} = 2H_{\mathrm{G}}$. With a little abuse of notation, we use 'inertia' to refer to M_{G}.

and 6 transmission lines, as well as Primary Frequency Control (PFC) and Automatic Voltage Regulation (AVR). Base-case data are given in [18].

All simulations were carried out using Dome [19] and were executed on a 64-bit Linux Ubuntu 18.04 operating system running on an 8 core 3.40 GHz Intel© Core i7™ with 16 GB of RAM.

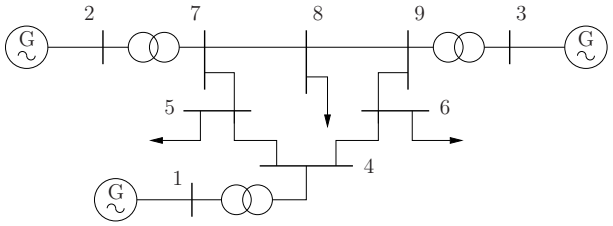

Fig. 4: WSCC 9-bus system utilized in the illustrative examples.

A. System Admittance Matrix

Due to its relevance for the remainder of this section, the matrix $\mathbf{B}_{\rm bus} = {\rm Im}\{\bar{\mathbf{Y}}_{\rm bus}\}$ of the WSCC grid is shown in Table I. Shunt capacitive charging of transmission lines is not needed for the calculation of the RoCoP $\dot{p}'_{{\rm B},h}(t)$, as justified in Section III, and are not included in $\mathbf{B}_{\rm bus}$.

TABLE I: WSCC system – Matrix $\mathbf{B}_{\rm bus}$.

Bus #	**Bus #**								
	1	2	3	4	5	6	7	8	9
1	–17.36	0	0	17.36	0	0	0	0	0
2	0	–16.00	0	0	0	0	16.00	0	0
3	0	0	–17.06	0	0	0	0	0	17.06
4	17.36	0	0	–39.47	11.60	10.51	0	0	0
5	0	0	0	11.60	–17.58	0	5.975	0	0
6	0	0	0	10.51	0	–16.98	0	0	5.588
7	0	16.00	0	0	5.975	0	–35.68	13.70	0
8	0	0	0	0	0	0	13.70	–23.48	9.784
9	0	0	17.06	0	0	5.588	0	9.784	–32.43

B. Local Bus Frequency Estimation

Bus frequencies are estimated with Synchronous Reference Frame PLLs (SRF-PLLs) whose model is described in several references, e.g. [20]. The fundamental-frequency model of an SRF-PLL is depicted in Fig. 5, which consists of a phase detector that is modeled as a lag transfer function; a loop filter that is a PI controller; and a voltage-controlled oscillator that is implemented as an integrator. In this scheme, $\theta_{{\rm B},h}(t)$ is the phase angle of the bus voltage phasor at bus h, and $\tilde{\theta}_{{\rm B},h}(t)$ is the corresponding estimated quantity. The output of the loop filter is an estimation of the frequency deviation $\Delta\tilde{\omega}_{{\rm B},h}(t)$ at the bus and is used in the simulations discussed below.

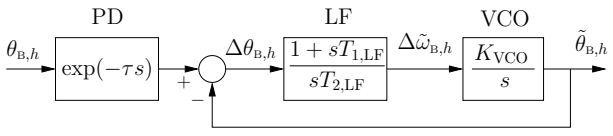

Fig. 5: Scheme of the SRF-PLL.

The need for precise frequency measurements may appear as a limitation of the proposed technique. However, in recent years, the accuracy and precision of frequency measurements has been improved significantly. In this paper we only consider frequency estimation based on PLLs, as these are ubiquitous in power converters [21], [22]. While it is known that, in some cases, PLLs can create dynamic issues, e.g. [23], [24], other promising methods, in particular those based on some variant of interpolated Discrete Fourier Transform (DFT) have been recently shown to be very precise. The interested reader can find a discussion on this approach in [17], [25] and in the references therein. Also the calculation of the rate of change of frequency has been largely investigated in recent years. Reference [26] provides, along with its own contributions, an introduction to the topic.

C. Synchronous Machine

The features of the proposed RoCoP index $\dot{p}'_{{\rm B},h}(t)$ are first tested considering the base-case scenario with inclusion of an Automatic Generation Control (AGC) implemented as a perfect tracking integral controller.

1) Comparison with Loads: Figure 6 shows the RoCoP for the generator connected to bus 3 and the load connected to bus 8 following the outage of 20% of the load connected to bus 5. Dropping for simplicity the dependency on time, the RoCoP of buses 3 and 8 are given by the following expressions based on (20):

$$\begin{aligned}\dot{p}'_{{\rm B},3} &= 17.06\,\Delta\tilde{\omega}_{{\rm B},3} - 17.06\,\Delta\tilde{\omega}_{{\rm B},9}\\ \dot{p}'_{{\rm B},8} &= 23.48\,\Delta\tilde{\omega}_{{\rm B},8} - 13.7\,\Delta\tilde{\omega}_{{\rm B},7} - 9.784\,\Delta\tilde{\omega}_{{\rm B},9}\ ,\end{aligned} \tag{40}$$

where the coefficients are obtained from Table I, and the symbol '$\sim$' on top of a bus frequency represents estimated values from the SRF-PLL. As thoroughly discussed in [10], for practical applications, if a measurement is not available, this can be calculated using measurements from other buses. For example, if there is no PMU at bus 3, $\Delta\tilde{\omega}_{{\rm B},3}$ can be replaced in (40) with:

$$\Delta\tilde{\omega}_{{\rm B},3} = \frac{32.43}{17.06}\,\Delta\tilde{\omega}_{{\rm B},9} - \frac{5.588}{17.06}\,\Delta\tilde{\omega}_{{\rm B},6} - \frac{9.784}{17.06}\,\Delta\tilde{\omega}_{{\rm B},8}, \tag{41}$$

which can be readily deduced from the last row of Table I.

Simulation results show that, as expected, at the generator bus, $\dot{p}'_{{\rm B},3}(t) \neq 0$ after the load outage, whereas, at the load bus, $\dot{p}'_{{\rm B},8}(t) \approx 0, \forall t$. The spike at beginning of the simulation of the load bus is due to the numerical integration of the SRF-PLL, and does not represent any physical behavior of the system.

In steady state, the index $\dot{p}'_{{\rm B},h}(t)$ is null, which indicates that, in stationary conditions, all machines rotate at the same speed and that all frequency controllers are inactive.

2) Layers of Frequency Control: Figure 7 shows the effect of removing the AGC from the system as well as the PFC from the generator at bus 3. The effect of the AGC on the RoCoP and the estimated power injection is negligible. This result is consistent with the transient nature of the RoCoP. On the other hand, if the PFC is disabled, the effect on the RoCoP is evident a few seconds after the contingency. In the first instants, the response of the RoCoP is driven exclusively by the inertia of the machine, as the three trajectories are

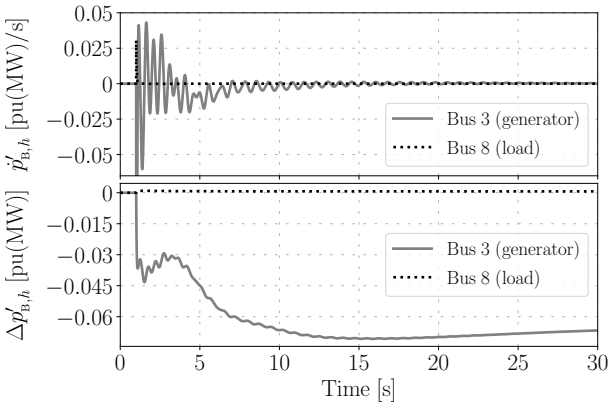

Fig. 6: WSCC system – Proposed RoCoP $\dot{p}'_{\mathrm{B},h}(t)$ and estimated variations of power injection at buses 3 (generator) and 8 (passive load).

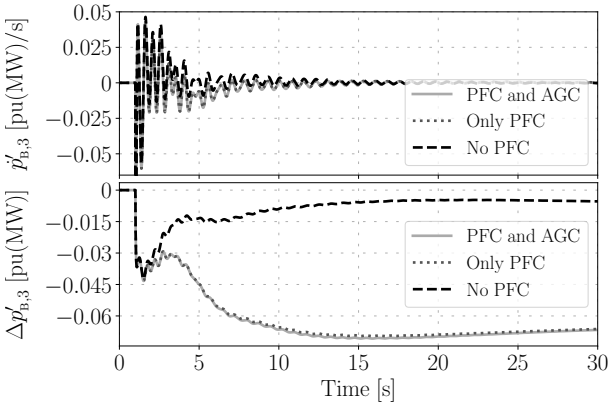

Fig. 7: WSCC system – Proposed RoCoP $\dot{p}'_{\mathrm{B},3}(t)$ and estimated variations of power injection at generation bus 3 for various frequency controls.

fairly similar up to about 2 seconds after the loss of the load. This property can be exploited to estimate accurately the inertia of the machines regardless of the type of frequency control to which the machines are coupled, as discussed in Subsection V-C.6.

3) Actual vs Regulating Active Power Injection: The estimated power injection at bus 3 shown in the bottom panels of Figs. 6 and 7 indicates that there is a jump in the trajectory of the active power generated by the SM. However, the turbine governors of SMs require several seconds to vary their mechanical power generation to match the power unbalance that, in this case, is due to the loss of part of the load at bus 5. This is graphically represented in Fig. 8, where the estimated $\Delta p'_{\mathrm{B},3}(t)$ is compared with the variations of the actual active power generated by the SM at bus 3 for the cases without any frequency control, and with both PFC and AGC.

Results shown in Fig. 8 indicate that the estimated $\Delta p'_{\mathrm{B},3}(t)$ includes the effect of the (fast) inertial response of the machine, $M_{\mathrm{G}}\dot{\omega}_{\mathrm{G}}(t)$, and the PFC, $p_{\mathrm{PFC}}(t)$. In Fig. 8, $\Delta p'_{\mathrm{B},3}(t)$ is calculated using (33), whereas the variation of the total power injection at the generator bus is $\Delta p_{\mathrm{B},3}(t) = p_{\mathrm{B},3}(t) - p_{\mathrm{B},3o}$. The actual variations of the mechanical power of the SM are smooth even in the first instants after the contingency, and following later a similar behavior than that estimated by the

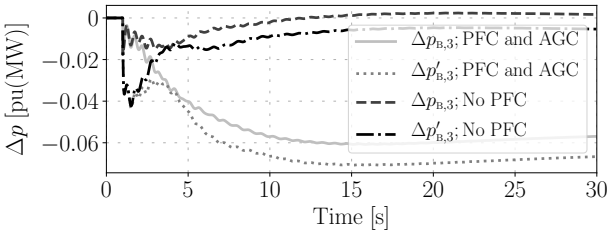

Fig. 8: WSCC system – Variations of the active power injected to bus 3 and regulating power for various frequency controls.

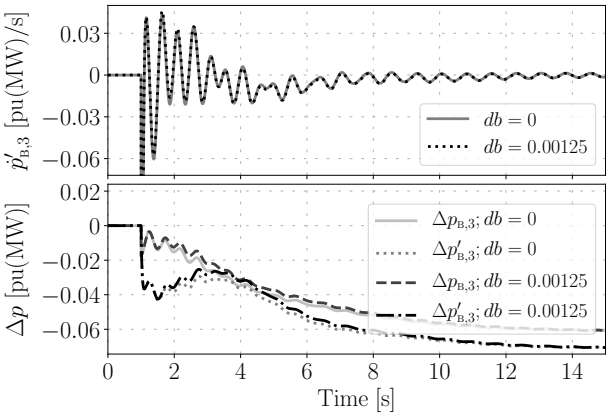

Fig. 9: WSCC system – Proposed RoCoP $\dot{p}'_{\mathrm{B},3}(t)$; and variations of the active power injected to bus 3 and regulating power with and without deadband in the turbine governor input signal.

regulating power $\Delta p'_{\mathrm{B},3}(t)$, i.e. after the inertial response of the SM gives way to the PFC.

4) Impact of Deadbands in the Turbine Governor: Turbine governors of SMs usually include deadbands on their frequency error input signal to *minimize generator movement due to frequency regulation* [27]. Therefore, the inclusion of this deadband results in a reduction of the sensitivity of the PFC on unbalances in the system, thus impacting on the variations of the power injected by the generators after a disturbance. Usually, the value of the deadband is designed to neglect *small* frequency variations due to, e.g., small load fluctuations or generation variability of renewable sources, and is of the order of a few tens tens of millihertzs.

For the sake of illustration, a deadband of 75 mHz (0.00125 pu) is considered in the example shown in Fig. 9, where the case from the previous section with PFC and AGC is simulated. The inclusion of the deadband reduces the variations of active power injected by the SM. This reduction is properly captured by the estimated regulating power, indicating that the accuracy of the estimation is not affected by the inclusion of the deadband.

5) Short-circuit Analysis: As discussed previously in Section V-B, accurate measurement of the frequency are required for the practical application of the technique proposed in this paper, which can pose some limitations, specially if fast events are registered such as short-circuits and line outages. This paper considers the well-known and ubiquitous SRF-PLL for estimating the frequency at a specific bus based on the processing of the bus voltage phase angle. It is also well-known that SRF-PLLs are prone to numerical issues and thus

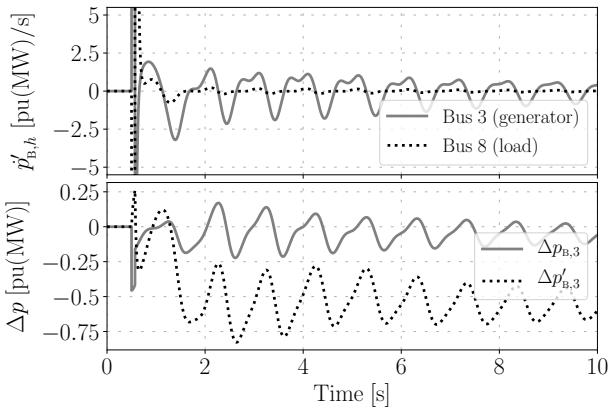

Fig. 10: WSCC system – Proposed RoCoP at buses 3 (generator) and 8 (load); and variations of the active power injected to bus 3 and regulating power following a three-phase fault cleared by the opening of the faulted line.

to measurement inaccuracies if such a phase angle experiences sudden jumps due to, e.g., the fast events discussed above, as well as other phenomena such as signal noise. In this illustrative example, the accuracy of the proposed RoCoP is studied when the system faces a short-circuit, cleared by the opening of the faulted line. An in-depth and thorough discussion on the effect of noise in the measured signal on the accuracy of the RoCoP is provided in the case study of Part II of this paper.

In this example, a three-phase fault is simulated at bus 7, which is cleared after 70 ms by opening the line connecting buses 7 and 5. The RoCoP at buses 3 and 8 is shown at the top panel of Fig. 10. The SRF-PLL causes spikes in the RoCoP which leads to peaks of $|\dot{p}'_{\mathrm{B},3}|_{\max} \approx 25$ and $|\dot{p}'_{\mathrm{B},8}|_{\max} \approx 100$. However, such spikes last for about the duration of the fault, i.e., around 100 ms. After such time, the RoCoP is able to accurately track the electromechanical oscillations of the machine, whereas it is virtually constant and equal to zero for the case of the load.

The small-amplitude oscillations of $\dot{p}'_{\mathrm{B},8}(t)$ in the first second after the fault clearance require a brief explanation. When the fault occurs and then when it is cleared, the bus voltage phase angles jump with different amplitudes at different buses. This means that the PLLs will recover an accurate estimation of the frequency with a lag that is different from bus to bus. The oscillations of $\dot{p}'_{\mathrm{B},8}(t)$ are thus due to the offset between the PLL frequency estimations at buses 7, 8 and 9 following the fault.

The bottom panel of Fig. 10 shows the variations of the injected and regulating active power at bus 3. During the first seconds after the contingency, the dominant component of the regulating power is not the active power injected by the machine, but the machine inertia, as discussed in equation (37). This causes a drift between both trajectories in the plot. After approximately $t = 2$ s, the effect of the inertia diminishes, being replaced by the active power variations due to the PFC. Note that the effect of the inertia does not *vanish* completely after such 2 seconds. The amplitude of $\Delta p'_{\mathrm{B},3}(t)$ is appreciably larger than that of $\Delta p_{\mathrm{B},3}(t)$ during the whole simulation. This

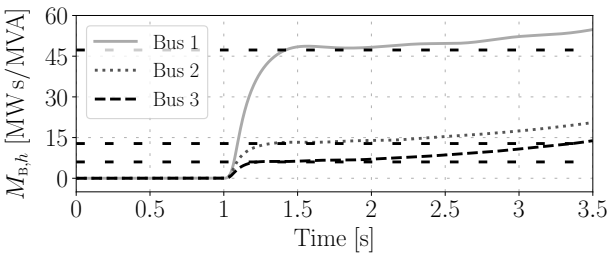

Fig. 11: WSCC system – Estimated inertia of the three synchronous machines. Dashed lines represent their actual inertia constants.

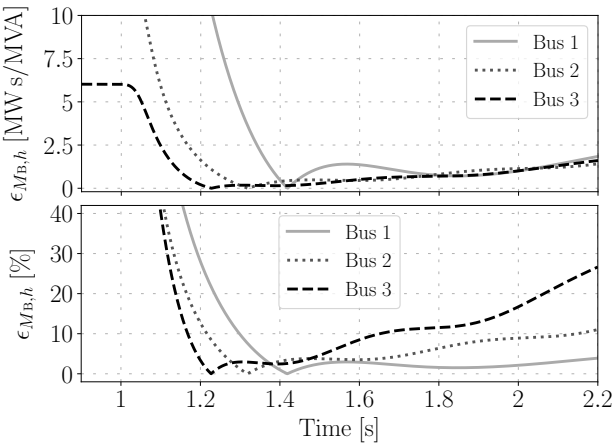

Fig. 12: WSCC system – Absolute and percentage inertia estimation errors of the three synchronous machines.

indicates that the inertia is naturally contributing during the oscillatory process.

6) Inertia Estimation: This example illustrates the expression (32) derived in Subsection IV-C to estimate the equivalent inertia of a device/subsystem. The estimated inertia of the three SMs of the system for the case with only PFC is shown in Fig. 11. The estimations are compared with their actual inertia constant, represented by the dashed horizontal lines, and whose values are $M_{\mathrm{G},1} = 47.28$, $M_{\mathrm{G},2} = 12.8$ and $M_{\mathrm{G},3} = 6.02$ MW s/MVA. Low-Pass Filters (LPFs) with time constant of 1 s have been added to the PLLs utilized to estimate bus frequencies for the three machines to clean the signals from numerical issues due to the sudden jumps of $\dot{p}'_{\mathrm{B},h}(t)$.

Results show that, in the first seconds after the contingency, the estimation of the machine inertias is highly accurate. Then, the trajectories drift away from their respective actual values due to the effect of the PFC of the generators.

As discussed in the previous example, the inertial response of synchronous machines is dominant during the first instants after a contingency (generally ≤ 1 sec). It is in this time window where the proposed technique can be used to estimate the device inertia based exclusively on local power and frequency measurements. This is shown in Fig. 12 below, where the absolute and percentage errors of the inertia estimation depicted in Fig. 11 are represented.

The estimation errors for the three machines have similar absolute values. This leads to smaller percentage errors for larger machines, which is to be expected as small machines are

more affected by the behavior of rest of the system, making more difficult the isolation of the individual impact of such a machine/device. Nevertheless, in the first 600 ms after the estimation fall time (in between 200 and 400 ms depending on the machine), the percentage inertia estimation error is, from larger to smaller machine, of $<3\%$, $<8\%$ and $<11\%$.

Note also that inertia is a fixed parameter of the machine/device, thus being able to estimate its value in the time frame of one second after a contingency will suffice, even though the accuracy of such an estimation is gradually declining with time while the primary frequency control takes part.

VI. Summary of Theoretical Results

The main theoretical results discussed in the first part of this paper are as follows.

- Starting from the well-known dc power flow formulation, we have deduced an alternative formulation of the FDF and formulated the link between the RoCoP injected into buses and bus frequency deviations. This results in the expressions (12) and (20).
- An empirical criterion to distinguish between devices that modify the frequency from those who do not is based on the RoCoP. This requires the definition of a threshold ϵ, determined based on the statistical properties of the device to be monitored. The device is able to modify the frequency at its point of connection with the grid only if $|\dot{p}'_{\mathrm{B},h}(t)| > \epsilon$. This criterion can be utilized to properly reward the ancillary services of synchronous and non-synchronous devices that provide primary frequency control.
- An approximated expression to evaluate, during a transient, the equivalent inertia of a device is given in (38). This expression can be utilized to quantify the inertial response provided by non-synchronous devices.

A relevant application of the theory discussed above to determine the frequency regulation support provided by non-synchronous devices is discussed in Part II of this paper.

Appendix

This appendix shows that the quota of active power that is defined as $p''_{\mathrm{B},h}(t)$ in (7), namely:

$$dp''_{\mathrm{B},h} = \sum_{k\in\mathbb{B}} \frac{\partial p_{\mathrm{B},h}}{\partial v_{\mathrm{B},k}}\, dv_{\mathrm{B},k}\,, \tag{42}$$

is the quota of the power associated with passive devices, such as constant admittances. We prove this statement using the limit case, i.e., we assume that the power consumed at bus h is that of a constant admittance and we deduce that, for this kind of device, $p'_{\mathrm{B},h}(t) = 0$.

Let us start from the expressions of the active and reactive power injections at bus h. For the sake of simplicity but without loss of generality, we assume that bus h is connected to the rest of the grid through only one bus, say bus k, and that the branch connecting the two buses is lossless, i.e., $G^{hk}_{\mathrm{bus}} = 0$. With these assumptions and according to the notation of (7), we have:

$$\begin{aligned} p_{\mathrm{B},h}(t) &= -G_h v^2_{\mathrm{B},h}(t) \\ &= v_{\mathrm{B},h}(t) v_{\mathrm{B},k}(t) B_{hk} \sin\theta_{\mathrm{B},hk}(t)\,, \end{aligned} \tag{43}$$

$$\begin{aligned} q_{\mathrm{B},h}(t) &= -B_h v^2_{\mathrm{B},h}(t) \\ &= B_{hk} v^2_{\mathrm{B},h}(t) - v_{\mathrm{B},h}(t) v_{\mathrm{B},k}(t) B_{hk} \cos\theta_{\mathrm{B},hk}(t)\,, \end{aligned} \tag{44}$$

where G_h and B_h are the conductance and the susceptance of the load and $B_{hk} = 1/X_{hk}$, where X_{hk} is the reactance of the branch connecting buses h and k.

Equation (44) can be rewritten as:

$$(B_h + B_{hk}) v^2_{\mathrm{B},h}(t) = v_{\mathrm{B},h}(t) v_{\mathrm{B},k}(t) B_{hk} \cos\theta_{\mathrm{B},hk}(t)\,. \tag{45}$$

Then squaring and adding (43) and (45), one obtains:

$$\tilde{B}^2_h v^4_{\mathrm{B},h}(t) = B^2_{hk} v^2_{\mathrm{B},h}(t) v^2_{\mathrm{B},k}(t)\,, \tag{46}$$

where $\tilde{B}^2_h = G^2_h + (B_h + B_{hk})^2$, or, equivalently:

$$\tilde{B}_h v_{\mathrm{B},h}(t) = B_{hk} v_{\mathrm{B},k}(t)\,, \tag{47}$$

or, equivalently:

$$v_{\mathrm{B},k}(t) = \frac{\tilde{B}_h}{B_{hk}}\, v_{\mathrm{B},h}(t)\,. \tag{48}$$

Substituting (48) in (43), we obtain:

$$-G_h v^2_{\mathrm{B},h}(t) = \tilde{B}_h v^2_{\mathrm{B},h}(t) \sin\theta_{\mathrm{B},hk}(t)\,, \tag{49}$$

or, equivalently:

$$\sin\theta_{\mathrm{B},hk}(t) = -\frac{G_h}{\tilde{B}_h} = \text{constant}\,, \tag{50}$$

which implies that, for a constant admittance load, $\theta_{\mathrm{B},hk}(t)$ is constant, but then $d\theta_{\mathrm{B},hk} = 0$ and, hence, by definition, $dp'_{\mathrm{B},h} = 0$ or, equivalently, $dp_{\mathrm{B},h} \equiv dp''_{\mathrm{B},h}$. □

It is relevant to observe that (50) also implies that $d\theta_{\mathrm{B},h} = d\theta_{\mathrm{B},k}$ or, equivalently, $\omega_{\mathrm{B},h}(t) = \omega_{\mathrm{B},k}(t)$. This confirms the assumption made in [8] in the definition of the frequency divider formula (4), where passive loads were assumed not to modify the frequency at their point of connection with the grid. The interested reader can find a discussion on the relation among $p_{\mathrm{B},h}(t)$, $p'_{\mathrm{B},h}(t)$ and $p''_{\mathrm{B},h}(t)$ for voltage-dependent loads and their ability to modify the frequency at their point of connection in [28].

References

[1] H. F. Illian, "Frequency control performance measurement and requirements," Lawrence Berkeley National Laboratory, Berkeley, Tech. Rep. LBNL-4145E, 2010.

[2] C. S. Xue and M. Martinez, "Review of the recent frequency performance of the Eastern, Western and ERCOT interconnections," Lawrence Berkeley National Laboratory, Berkeley, Tech. Rep. LBNL-4144E, 2010.

[3] F. Milano, F. Dörfler, G. Hug, D. J. Hill, and G. Verbič, "Foundations and challenges of low-inertia systems (invited paper)," in *Power Systems Computation Conference (PSCC)*, Dublin, Ireland, Jun. 2018, pp. 1–25.

[4] J. H. Eto, J. Undrill, P. Mackin, R. Daschmans, B. Williams, B. Haney, R. Hunt, J. Ellis, H. Illian, C. Martinez, M. O'Malley, K. Coughlin, and K. Hamachi LaCommare, "Use of frequency response metrics to assess the planning and operating requirements for for reliable integration of variable renewable generation," Lawrence Berkeley National Laboratory, Berkeley, Tech. Rep. LBNL-4145E, 2010.

[5] P. Du and Y. Makarov, "Using disturbance data to monitor primary frequency response for power system interconnections," *IEEE Trans. on Power Systems*, vol. 29, no. 3, pp. 1431–1432, May 2014.
[6] P. Du and J. Matevosyan, "Forecast system inertia condition and its impact to integrate more renewables," *IEEE Trans. on Smart Grid*, vol. 9, no. 2, pp. 1531–1533, Mar. 2018.
[7] P. Bhui, N. Senroy, A. K. Singh, and B. C. Pal, "Estimation of inherent governor dead-band and regulation using unscented Kalman filter," *IEEE Trans. on Power Systems*, vol. 33, no. 4, pp. 3546–3558, Jul. 2018.
[8] F. Milano and Á. Ortega, "Frequency divider," *IEEE Trans. on Power Systems*, vol. 32, no. 2, pp. 1493–1501, Mar. 2017.
[9] J. Zhao, L. Mili, and F. Milano, "Robust frequency divider for power system online monitoring and control," *IEEE Trans. on Power Systems*, vol. 33, no. 4, pp. 4414–4423, Jul. 2018.
[10] F. Milano, Á. Ortega, and A. J. Conejo, "Model-agnostic linear estimation of generator rotor speeds based on phasor measurement units," *IEEE Trans. on Power Systems*, vol. 33, no. 6, pp. 7258–7268, Nov. 2018.
[11] F. Milano, "Rotor speed-free estimation of the frequency of the center of inertia," *IEEE Trans. on Power Systems*, vol. 33, no. 1, pp. 1153–1155, Jan 2018.
[12] B. Stott, J. Jardim, and O. Alsac, "DC power flow revisited," *IEEE Trans. on Power Systems*, vol. 24, no. 3, pp. 1290–1300, Aug. 2009.
[13] F. Bouffard, F. D. Galiana, and A. J. Conejo, "Market-clearing with stochastic security-part I: formulation," *IEEE Trans. on Power Systems*, vol. 20, no. 4, pp. 1818–1826, Nov. 2005.
[14] F. Milano and R. Zárate Miñano, "A systematic method to model power systems as stochastic differential algebraic equations," *IEEE Trans. on Power Systems*, vol. 28, no. 4, pp. 4537–4544, Nov 2013.
[15] EirGrid, SONI, "Quarterly wind dispatch down report user guide." [Online]. Available: http://www.eirgridgroup.com
[16] R. Zárate Miñano and F. Milano, "Construction of SDE-based wind speed models with exponentially decaying autocorrelation," *Renewable Energy*, vol. 94, pp. 186 – 196, 2016.
[17] A. Derviškadić, P. Romano, and M. Paolone, "Iterative-interpolated DFT for synchrophasor estimation: A single algorithm for P- and M-class compliant PMUs," *IEEE Trans. on Instrumentation and Measurement*, vol. 67, no. 3, pp. 547–558, March 2018.
[18] P. W. Sauer and M. A. Pai, *Power System Dynamics and Stability*. Upper Saddle River, NJ: Prentice Hall, 1998.
[19] F. Milano, "A Python-based software tool for power system analysis," in *Procs of the IEEE PES General Meeting*, Vancouver, BC, July 2013.
[20] G.-C. Hsieh and J. C. Hung, "Phase-Locked Loop Techniques – A Survey," *IEEE Trans. on Industrial Electronics*, vol. 43, no. 6, pp. 609–615, Dec. 1996.
[21] S. Wang, J. Hu, X. Yuan, and L. Sun, "On inertial dynamics of virtual-synchronous-controlled DFIG-based wind turbines," *IEEE Trans. on Energy Conversion*, vol. 30, no. 4, pp. 1691–1702, Dec 2015.
[22] J. Hu, S. Wang, W. Tang, and X. Xiong, "Full-capacity wind turbine with inertial support by adjusting phase-locked loop response," *IET Renewable Power Generation*, vol. 11, no. 1, pp. 44–53, 2017.
[23] Ö. Göksu, R. Teodorescu, C. L. Bak, F. Iov, and P. C. Kjær, "Instability of wind turbine converters during current injection to low voltage grid faults and PLL frequency based stability solution," *IEEE Trans. on Power Systems*, vol. 29, no. 4, pp. 1683–1691, July 2014.
[24] F. Bizzarri, A. Brambilla, and F. Milano, "Analytic and numerical study of TCSC devices: Unveiling the crucial role of phase-locked loops," *IEEE Trans. on Circuits and Systems I: Regular Papers*, vol. 65, no. 6, pp. 1840–1849, June 2018.
[25] P. Romano and M. Paolone, "Enhanced interpolated-DFT for synchrophasor estimation in FPGAs: Theory, implementation, and validation of a PMU prototype," *IEEE Trans. on Instrumentation and Measurement*, vol. 63, no. 12, pp. 2824–2836, Dec 2014.
[26] G. Frigo, A. Derviškadić, Y. Zuo, and M. Paolone, "PMU-based ROCOF measurements: Uncertainty limits and metrological significance in power system applications," *IEEE Trans. on Instrumentation and Measurement*, pp. 1–1, 2019.
[27] I. Abdur-Rahman, S. Niemeyer, and R. Vera, "Frequency regulation: Is your plant compliant?" *Power Engineering*, 2010, available at www.power-eng.com.
[28] Á. Ortega and F. Milano, "Estimation of voltage dependent load models through power and frequency measurements," *IEEE Trans. on Power Systems*, 2020, pre-print available on IEEExplore.ieee.org.

Federico Milano (S'02, M'04, SM'09, F'16) received from the University of Genoa, Italy, the ME and Ph.D. in Electrical Engineering in 1999 and 2003, respectively. From 2001 to 2002, he was with the Univ. of Waterloo, Canada. From 2003 to 2013, he was with the Univ. of Castilla-La Mancha, Spain. In 2013, he joined the Univ. College Dublin, Ireland, where he is currently Professor of Power Systems Control and Protections and Head of Electrical Engineering. His research interests include power systems modeling, control and stability analysis.

Álvaro Ortega (S'14, M'16) received the degree in Industrial Eng. from Escuela Superior de Ingenieros Industriales, Univ. of Castilla-La Mancha, Ciudad Real, Spain, in 2013. In 2017, he received the Ph.D. in Electrical Eng. from Univ. College Dublin, Ireland, where he stayed until 2019. In 2020, he joined the **LOYOLA**Tech institute in Universidad Loyola Andalucía, where he practices as senior power systems researcher. His current current fields of research include modeling, control and stability of energy storage systems; frequency estimation, control and stability in low-inertia systems; and design of advanced monitoring and control systems for flexible energy grids.